Modelling and control of a smart auxiliary mass damper equipped with a Bragg grating

Chris May* Aldo Minardo† Ciro Natale† Pietro Pagliarulo* Salvatore Pirozzi†
*Laboratory of Process Automation (LPA), Saarland University, Saarbrücken, Germany
†Department of Information Engineering, Second University of Naples, Aversa, Italy

***Abstract*— This paper presents the results of a key activity of a large research project in the aeronautics field, funded by the European Community under the Sixth Framework Programme, namely the modelling and control of a magnetostrictive actuator to be used for broadband vibration and noise control. The developed auxiliary mass damper is designed in order to meet the demanding requirements of the application at hand, especially in terms of weight reduction and force capability. The specifications are successfully satisfied using an inertial resonant actuator concept based on a nonlinear amplification mechanism of the seismic mass displacement. The nonlinearities of the actuator highly affect the problem of its adoption within the active feedback control system devoted to vibration and noise reduction of the controlled structure. In order to overcome the limitation and negative effects of these nonlinearities within the main control system, the actuator is equipped with an optical sensor based on a Bragg grating used for a low-level control loop aimed at imposing a desired linear behaviour to the actuator itself. A preliminary modelling and characterization of the dynamic behaviour of the actuator is performed taking into account also the hysteretic nonlinearity exhibited by the active material as well as the nonlinear dynamics of the mechanical actuator structure. A model-following control algorithm, designed on the basis of an experimentally identified dynamic model, is adopted as the low-level control algorithm. Experimental results show the effectiveness of the approach and its validity as the first step to be taken during the design phase of the complete noise and vibration control system.**

***Index Terms*— Smart actuator, Nonlinear behaviour, Model-following, Magnetostrictive material**

I. Introduction

The present work, which is part of the MESEMA project [6], [12], has the main objective of designing and implementing an active noise control system on a full-scale test rig consisting of a segment of a civil aircraft fuselage. The problem to be addressed is the reduction of cabin noise caused by turbulence induced vibrations on the fuselage exciting the skin panels. The typical "bump" noise is found in a broad frequency band ranging from 100 Hz to 400 Hz depending on the value of the trim velocity of the aircraft. The selected control strategy is based on a structural approach in which a large number of actuators with suitable force capability excite the structural elements of the fuselage in order to robustly counteract the vibration induced by the primary disturbance and thus the emitted noise. After a preliminary structural and acoustic analysis of the test article the actuator specifications have been derived in terms of required forces and maximum allowed weight. In detail, each actuator should be able to generate a force spectrum with a peak of 6 N at 130 Hz with a maximum weight of 150 g.

Based on a proven and patented actuator concept [13], the magnetostrictive auxiliary mass damper, shown in Fig. 1, was optimally designed for this application [14]. The dynamic behaviour of the smart auxiliary mass damper depends strongly on two sources of nonlinearity. The first one is due to the elastic suspension kinematics used for displacement amplification; the second one is due to the hysteretic behaviour of the magnetostrictive material. As reported in [3], the latter nonlinear effect can be compensated to improve the performance of the smart auxiliary mass damper when the actuator is used in a feedback control system. This compensation has been successfully accomplished by means of an hysteresis inversion algorithm [9], [10] implemented on an FPGA based hardware platform as detailed in [7]. The kinematic nonlinearity results in a shift of the actuator's resonant frequency with respect to the driving current amplitude. This nonlinear dynamic behaviour not only complicates the use of the actuator in the noise control system but also prevents the actuator from delivering the required force at the desired frequency. So it is fundamental to implement a low-level control algorithm able to fix the actuator resonant frequency. A model-following control strategy [1] which makes use of the measured displacement of the actuator seismic mass has been selected. The characteristic of the model-following algorithm consists in preserving the nature of the input signal of the low-level control system, which is the output of the high-level noise control system. A novel sensor based on a fibre Bragg grating (FBG) has been specially designed for measurement of the actuator displacement.

Due to their fibre-based, highly localized and wavelength encoded operation, FBGs offer attractive sensing possibilities, especially in strain and temperature embedded sensing of smart structures [8]. FBGs are low-weight, small-size sensors, and they can be easily attached to any material. Moreover, due to their dielectric nature, FBGs are immune to electromagnetic irradiation. This was of particular importance in our work, as the magnetostrictive nature of the actuator would be a source of disturbances in electrical-based or magnetic-based sensors. FBGs can be usefully employed as both static and dynamic sensors. In particular, the possibility to employ Bragg gratings to measure dynamic strains, has been widely demonstrated [17], [4], [2]. Also multi-point dynamic strain sensing has been reported, by using multiplexing schemes based on wavelength division and/or

1-4244-1264-1/07/$25.00 ©2007 IEEE

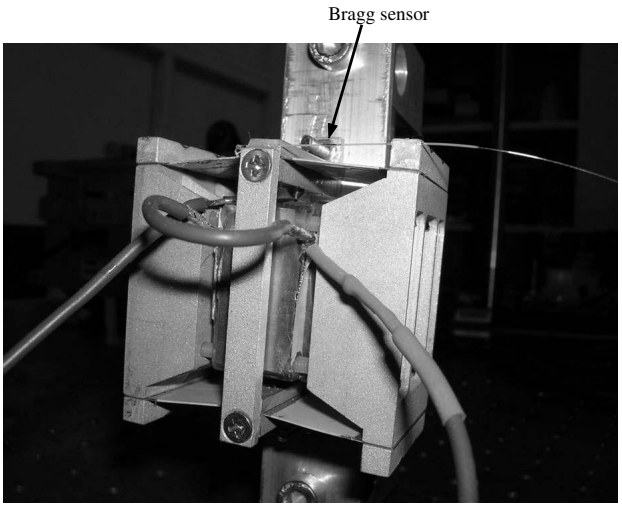

Fig. 1. Smart auxiliary mass damper.

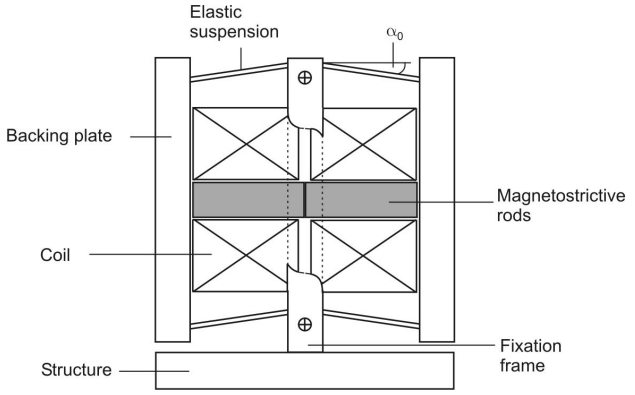

Fig. 2. Schematic design of the smart auxiliary mass damper.

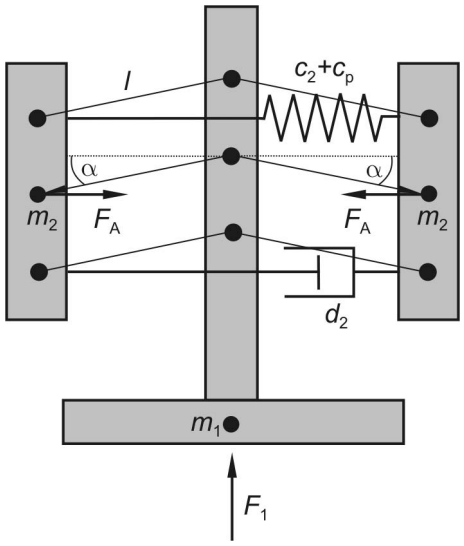

Fig. 3. Schematic diagram of the actuator mechanics.

time division [15], [18]. The use of multiplexing techniques permits interrogating multiple FBGs written on the same optical fibre, with a modest increase of the system cost with respect to a single-FBG interrogation set-up. In the present work, a single FBG was mounted on the magnetostrictive actuator in order to measure the displacement of the actuator itself. Interrogation of the FBG was carried out by using the narrow-band demodulation technique [19], which will be described in the following.

The effectiveness of the proposed strategy to control the smart actuator has been demonstrated through experiments whose results show that the controlled auxiliary mass damper has a resonance fixed at the desired frequency value. Future work will be devoted to using the controlled actuators within the complete noise control system.

II. Actuator description and modelling

Fig. 2 shows the fundamental construction inside the smart auxiliary mass damper [13]. It consists of magnetostrictive rods surrounded by two coils. The coils are on two backing plates that are connected with the stiff frame via two elastic suspensions arranged in parallel. The frame itself is mounted to the vibrating mechanical structure. Due to the magnetostrictive effect a magnetic field caused by a driving current $I(t)$ in the coils produces a small extension $s_A(t)$ in the magnetostrictive rods in the horizontal direction. This extension is transformed by the elastic suspensions to a significantly larger motion of the total mass –consisting of the magnetostrictive rods, the coils and the backing plates– in the perpendicular direction. The displacement amplification decisively depends on the angle of the elastic suspension at the working point α_0 of the mechanical construction (see Fig. 2) and is greater the smaller this angle α_0 is chosen. As a result of Newton's second law, the total moved mass produces an inertial force that has an effect on the vibrating mechanical structure [13], [14], [16], [11].

A. Nonlinear dynamics

The displacement amplification is represented in a first approximation by two parallel rigid arms of length l suspended at play-free and frictionless joints (see Fig. 3).

The elasticity of the suspension and the mechanical preload spring for the actuator are considered by the linear elastic spring with stiffness c_2. The structural damping in this construction is described by the linear viscous damper with damping d_2. The masses of the backing plates, coils as well as of the moving portions of the suspension and the active material are concentrated in the two identical masses m_2, so that the moved auxiliary mass consists of $2m_2$. The mass m_1 describes the effective mass of the structure to be dampened. The spring with stiffness c_p and the active force F_A describe the passive mechanical behaviour of the active component. The force F_1 represents the unknown disturbance at the point of the structure whose oscillations are to be reduced.

The state variables are the suspension angle $\alpha(t)$ and the angular velocity $\omega(t)$. A nonlinear mathematical model in state space was derived according to the Lagrange formal-

ism [5]. The state space equations are

$$\dot{\omega} = -n_1(\alpha)\omega^2 - n_2(\alpha)\omega - n_3(\alpha,\alpha_0) - n_4(\alpha)s_A + n_5(\alpha)F_1 \quad (1)$$

$$\dot{\alpha} = \omega \quad (2)$$

with

$$n_1(\alpha) = \frac{2m_2 \sin\alpha\cos\alpha}{m_1 + 2m_2\sin^2\alpha}$$

$$n_2(\alpha) = \frac{2d_2(m_1+2m_2)\sin^2\alpha}{m_2(m_1+2m_2\sin^2\alpha)}$$

$$n_3(\alpha,\alpha_0) = \frac{2(c_2+c_p)(m_1+2m_2)(\cos\alpha_0 - \cos\alpha)\sin\alpha}{m_2(m_1+2m_2\sin^2\alpha)}$$

$$n_4(\alpha) = \frac{c_p(m_1+2m_2)\sin\alpha}{lm_2(m_1+2m_2\sin^2\alpha)}$$

$$n_5(\alpha) = \frac{\cos\alpha}{l(m_1+2m_2\sin^2\alpha)}$$

This nonlinear model is able to reproduce the typical nonlinear effect of resonant frequency shifting with respect to input current amplitude, experimentally detected as shown in Fig. 4.

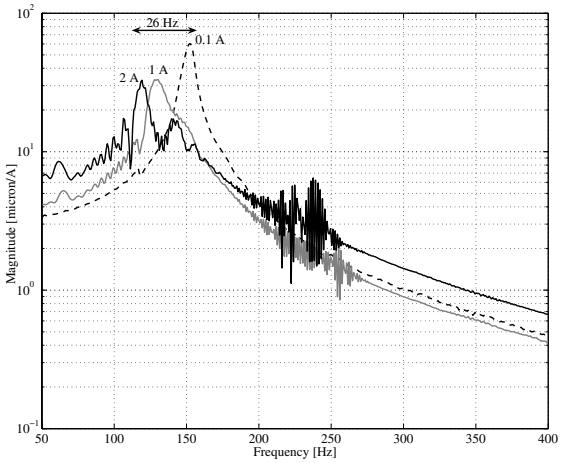

Fig. 4. Magnitude of frequency response function of the actuator for different current amplitudes.

B. Hysteresis model

The hysteretic behaviour of the magnetostrictive material can be modelled well with the modified Prandtl-Ishlinskii hysteresis operator that is represented by the following equation

$$\Gamma[x] = S[H[x]] \quad (3)$$

where H is a Prandtl-Ishlinskii hysteresis operator and S is a Prandtl-Ishlinskii superposition operator [9], [10], [16], [7]. In this way the relationship between the model input $s_A(t)$ and the control input, i.e. the driving current $I(t)$, is given by the equation

$$s_A(t) = \Gamma[I(t)] \quad (4)$$

As mentioned in the Introduction, this relationship can be inverted according to the method described in [9].

III. Optical sensor

A. FBG-based measurement scheme

In our set-up, dynamic strain measurements were carried out by employing a narrow-band demodulation scheme. The output light wave from a single longitudinal mode Distributed FeedBack (DFB) diode laser was used to probe the wavelength shift of the FBG reflection curve imposed by the strain signal to be detected. If the laser frequency is within the linear range of the FBG reflection slope, the strain signals will change the reflected power, which can be simply measured using a photodetector [19]. It can be seen that this technique has several advantages, such as low cost, fast response, and easy of use. The reflectivity spectrum of the FBG used in our experiments had a quasi-flat top from $1552\,\text{nm}$ to $1556\,\text{nm}$, with a peak reflectivity of $\geq 75\%$ (see Fig. 5). The leading edge of the FBG reflection curve extended from $1547.28\,\text{nm}$ to $1550.95\,\text{nm}$ (measured from 10% to 90% of maximum reflectivity), whereas the trailing edge extended from $1556.37\,\text{nm}$ to $1557.24\,\text{nm}$. The trailing edge of the FBG reflection curve allowed for a $72\,\text{GHz}$ linear slope width, and it was chosen as the operating range due to the higher linearity exhibited by the FBG reflectivity in this spectral portion. In order to keep a linear relationship between the reflected optical power and the strain signal, the DFB laser emitting wavelength must lie within the trailing edge of the FBG reflectivity spectrum (see Fig. 5). Moreover, assuming a typical FBG curve shift of $1\,\text{nm}$ for an applied strain of $1000\,\mu\epsilon$ [8], the strain level must be kept lower than $870\,\mu\epsilon$ in order to avoid sensor output saturation.

The optical set-up employed for FBG interrogation is schematically illustrated in Fig. 6. Light emitted by a DFB laser was sent to a Y-coupler, which directed the light to the FBG. Light reflected from the FBG was then re-directed to a photodiode, whose bandwidth was on the order of hundreds of MHz, thus much higher than the bandwidth of the strain signals to be detected. The output signal from the photodiode was finally sent to the conditioning electronics, basically comprised of a bandpass filter used to eliminate the dc component and high-frequency noise.

B. Mounting and calibration

Before attaching the FBG to the magnetostrictive actuator, the portion of fibre jacket corresponding to the grating position was removed, so as to avoid strain transfer loss from actuator to FBG. The FBG was then pre-stressed and glued to the actuator by epoxy resin (see Fig. 1). Pre-stressing of the FBG was necessary in order to avoid buckling of the fibre in which the sensor is written. Mounting of the FBG was carried out with the aim to measure one of the state variables of the system $\alpha(t)$. A sketch of the mounting set-up is shown in Fig. 7. As the output provided by the FBG is proportional to the strain of the fibre segment between the two bonding points A and B, the relationship between the strain and the angular displacement has to be determined. Such a relationship can be obtained by means of geometrical considerations. Referring to Fig. 7, let us start by considering that, under real experimental conditions, the displacement

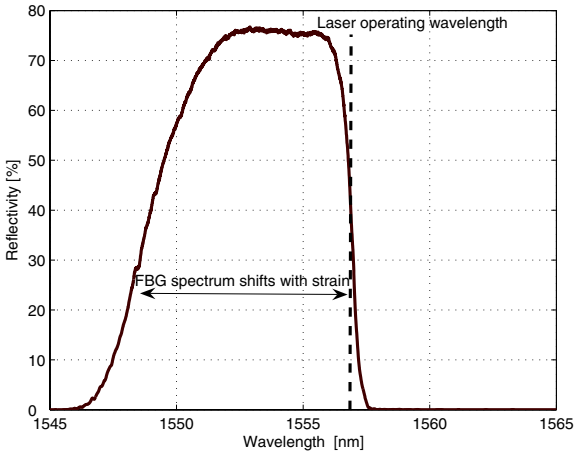

Fig. 5. Reflectivity spectrum of the grating.

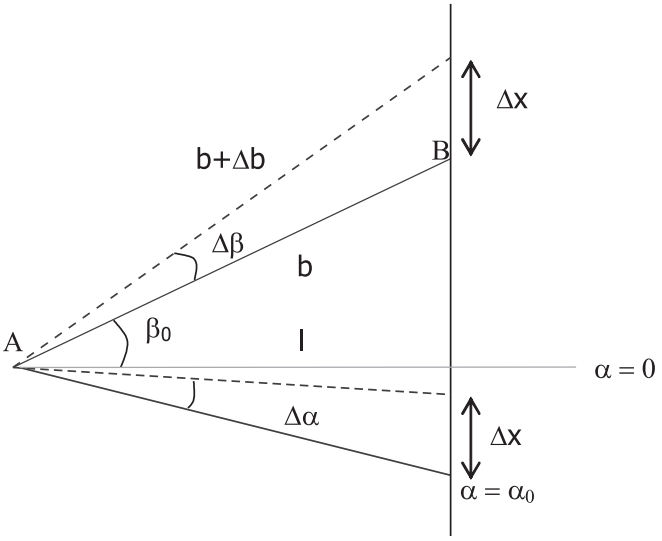

Fig. 7. Sketch of mounting setup.

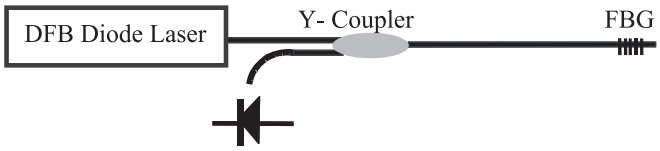

Fig. 6. FBG interrogation scheme.

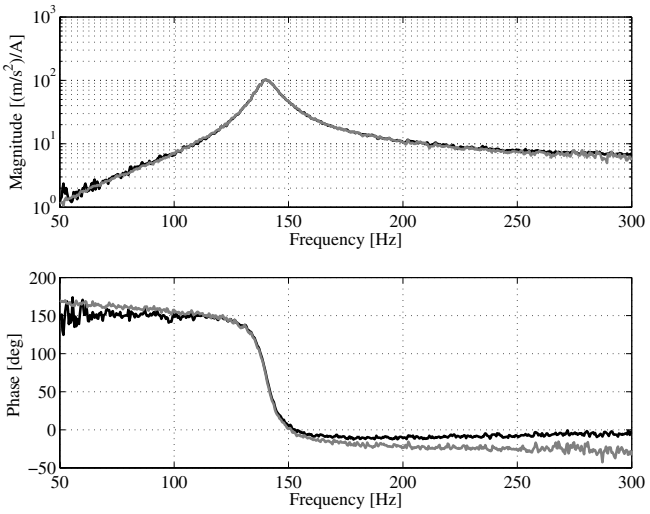

Fig. 8. Bragg calibration result: accelerometer (black), Bragg second time derivative (gray).

Δx of the moving mass is much smaller than the lever arm length l. Hence, $\Delta x \approx l\Delta\alpha$. Moreover, Δx is also much smaller than the fibre segment b, so that we can also assume $\Delta\beta \approx 0$. Under this approximation, the displacement Δx is nearly equal to Δb. As the optical output is proportional to the strain $\Delta b/b$, we can finally write

$$\epsilon \equiv \frac{\Delta b}{b} \approx \frac{l}{b}\Delta\alpha \tag{5}$$

Hence, under the small signal hypothesis, the quantity measured by the FBG is directly proportional to the angle variation $\Delta\alpha = \alpha - \alpha_0$. After bonding the FBG, the DFB laser output wavelength was temperature-tuned in order to guarantee a linear response of the sensor, over the whole range of actuator displacement. Calibration of the FBG was carried out by aid of an accelerometer mounted to the moving mass, so as to measure the acceleration along the vertical axis. The sensor sensitivity was estimated by comparing the measured frequency response functions from the excitation signal to the second time derivative of the FBG output signal, and from the excitation signal to the accelerometer output signal, respectively. Results are shown in Fig. 8. Based on the calibration constant of the accelerometer, we estimated an FBG sensitivity of about $37.6\,mV/\mu m$.

IV. Control strategy

As mentioned before, the actuator has a resonant frequency that shifts with respect to amplitude of the driving current. This nonlinearity affects the satisfaction of the force requirements and makes the actuator difficult to implement in the noise control system. Therefore, the low-level control objective is to fix the resonance of the actuator despite the amplitude of the input current.

First of all, a linear model reproducing the behaviour of the actuator in the neighborhood of a given working condition, i.e. with a given current amplitude and so with a fixed resonant frequency, is identified using a frequency domain identification procedure. It can be written in the classical state-space form as

$$\dot{x}(t) = Ax(t) + Bu(t) \tag{6}$$
$$y(t) = Cx(t) + Du(t) \tag{7}$$

where $u(t)$ is the actuator input current and $y(t)$ is the measured Bragg signal. The state equation (6) corresponds to the linearised version of the nonlinear model in Eq. (1),(2)

about the initial suspension angle α_0.

The adopted control strategy is based on a model-following approach [1] and the control scheme is reported in Fig. 9. The characteristic of the model-following algorithm consists in preserving the nature of the input signal of the control system. This makes the use of the actuator more transparent in the higher level control system computing the reference current for the actuator as a result of an outer feedback loop. This is accomplished by defining a reference model whose input is just the reference current $u_r(t)$ while the actuator input is the sum of the reference current and a corrective current $u_c(t)$ computed by the controller on the basis of the output error $e_y(t) = y(t) - y_r(t)$, $y_r(t)$ being the reference output. In particular, the reference model is selected equal to the identified linear model of the actuator, i.e.

$$\dot{x}_r(t) = Ax_r(t) + Bu_r(t) \quad (8)$$
$$y_r(t) = Cx_r(t) + Du_r(t) \quad (9)$$

As a consequence, the dynamics of the state error $e_x(t) = x(t) - x_r(t)$ is described by the state space representation

$$\dot{e}_x(t) = Ae_x(t) + Bu_c(t) \quad (10)$$
$$e_y(t) = Ce_x(t) + Du_c(t) \quad (11)$$

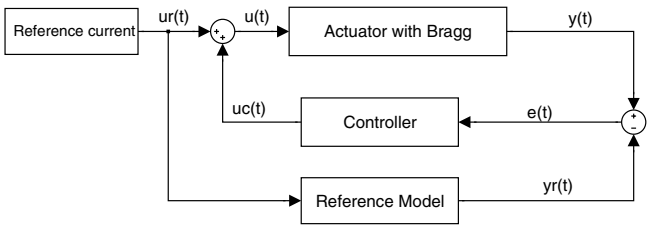

Fig. 9. Reference model control scheme.

Since the state e_x is obviously not accessible, the controller is designed according to a standard LQG procedure consisting of a Kalman filter as observer of the error dynamics and an optimal state feedback regulator. Therefore, its dynamic equations can be written in the form

$$\dot{x}_c(t) = A_c x_c(t) + B_c e_y(t) \quad (12)$$
$$u_c(t) = C_c x_c(t) \quad (13)$$

where $A_c = A - LC - BK + LDK$, $B_c = L$ and $C_c = -K$, with L and K being the solutions of the two classical Riccati equations.

V. Experimental results

The identification of the reference model has been carried out using FDIDENT, a MATLAB toolbox for identification in the frequency domain. The actuator has been excited with a chirp input current in the frequency range $[50, 600]$ Hz with amplitude 1 A, repeated 8 times, and the signal of the Bragg sensor has been acquired. Then, the frequency response function mapping current to the Bragg signal has been estimated with 8 averages to reduce noise effect and has been used as data input to the identification procedure. The reference model resulting from the identification is a sixth order model and the results of the model validation are shown in Fig. 10, where the measured and modelled frequency response functions are reported for comparison.

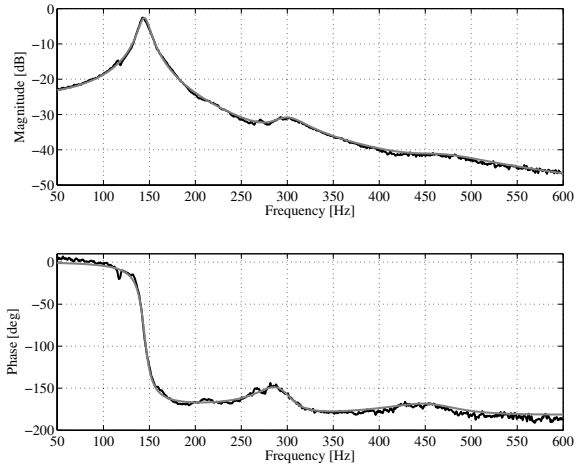

Fig. 10. Bode diagram of the identified reference model: modelled (gray) and measured (black).

The controller has been designed solving the LQG problem, with a process noise covariance matrix

$$Q = q_0 I + qB_r B_r^{\mathrm{T}} \quad (14)$$

with $q_0 = 1e-4$, I the identity matrix, $q = 0.5 \cdot 10^{-2}$, and as measurement noise covariance $v = 0.2 \cdot 10^{-3}$. The weights for the regulator problem have been chosen equal to $W = C^{\mathrm{T}}C$ as the state weight and $r = 0.1$ as the input weight. Fig. 11 reports the effect of the implemented controller on the resonant frequency of the actuator. It is evident that the resonance remains fixed even for different input current amplitudes when the closed-loop control is active. Of course, this result requires a control effort, in fact, for a reference current with an amplitude of 0.7 A, the total driving current has a peak up to 2 A, as shown in Fig. 12 where the black line represents the reference current and the gray line represents the total current. The offset current of 2 A is needed for the magnetic bias of the active material.

VI. Conclusions

A control algorithm based on a model-following approach has been applied to linearise the dynamic behaviour of a magnetostrictive auxiliary mass damper exhibiting kinematic and hysteretic nonlinearities. The inner control loop makes use of a strain sensor based on a fibre Bragg grating delivering a signal representing the displacement of the seismic mass of the device. In follow-up activities, the resulting linearised system will be implemented within an overall control system for lowering the sound pressure level in an aircraft cabin by resorting to a structural active control approach.

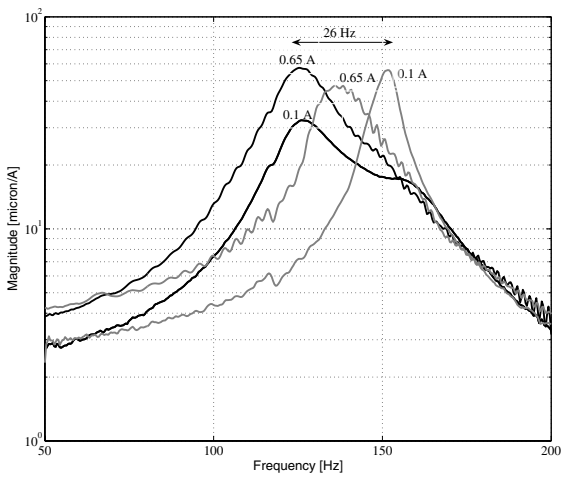

Fig. 11. Magnitude of the frequency response function of the actuator for different current amplitudes: open loop (gray) and closed loop (black)

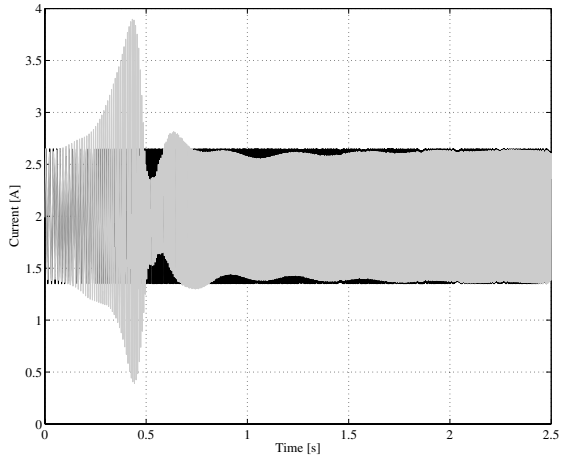

Fig. 12. Actuator current: open loop (black) and closed loop (gray).

ACKNOWLEDGMENTS

This paper was generated within the context of the MESEMA project, funded under the 6th Framework Programme of the European Community (Contract N. AST3-CT-2003-502915). The authors are solely responsible for its content, it does not represent the opinion of the European Community, and the Community is not responsible for any use that might be made of the information contained therein.

REFERENCES

[1] A. Balestrino, G. De Maria, and A. S. I. Zinober, "Nonlinear adaptive model-following control," *Automatica*, vol. 20, no. 5, pp. 559–568, 1984.

[2] D. C. Betz, G. Thursby, B. Culshaw, and W. J. Staszewski, "Acousto-ultrasonic sensing using fiber bragg gratings," *J. Smart Mater. Struct.*, vol. 12, pp. 122–128, 2003.

[3] A. Cavallo, N. C., S. Pirozzi, and C. Visone, "Effects of hysteresis compensation in feedback control systems," *IEEE Tran. on Magnetics*, vol. 39, no. 3.

[4] N. E. Fisher, D. J. Webb, C. N. Pannell, D. A. Jackson, J. W. Gavrilov, L. R.and Hand, L. Zhang, and I. Bennion, "Ultrasonic field and temperature sensor based on short in-fibre bragg gratings," *Electron. Lett.*, vol. 34, no. 11, pp. 1139–1140, 1998.

[5] H. Goldstein, C. P. J. Paole, and J. L. Safko, *Klassische Mechanik*, Wiley-VCH, Ed., Berlin, Germany, 2006.

[6] http://www.mesema.info.

[7] H. Janocha, D. Pesotski, and K. Kuhnen, "Fpga-based compensator of hysteretic actuator nonlinearities for highly dynamic applications," in *Proc. 10th International Conference on New Actuators*, Bremen, Germany, 2006, pp. 1013–1016.

[8] A. D. Kersey, M. A. Davis, H. J. Patrick, M. LeBlanc, K. P. Poo, A. G. Askins, M. A. Putnam, and E. J. Friebele, "Fiber grating sensors," *Journal of Lightw. Technol.*, vol. 15, no. 8, pp. 1442–1462, 1997.

[9] K. Kuhnen, "Modelling, identification and compensation of complex hysteretic nonlinearities - a modified prandtl-ishlinskii approach," *European Journal of Control*, vol. 9, no. 4, pp. 407–418, 2003.

[10] K. Kuhnen and H. Janocha, "Inverse feedforward controller for complex hysteretic nonlinearities in smart material systems," *Control and Intelligent System*, vol. 29, no. 3, pp. 74–83, 2001.

[11] K. Kuhnen, P. Pagliarulo, C. May, and H. Janocha, "Adaptronische schwingungsabsorber fr einen weiten einsatzbereich," *At-Automatisierungstechnik*, vol. 54, pp. 294–303, 2006.

[12] L. Lecce, E. Monaco, and F. Franco, "Mesema (magnetoelastic energy system for even more electric aircraft): Objectives and first results," in *Proc. 10th International Conference on New Actuators*, Bremen, Germany, 2006, pp. 936–939.

[13] C. May, K. Kuhnen, and H. Pagliarulo, P.and Janocha, "Magnetostrictive dynamic vibration absorber (dva) for passive and active damping," in *Proc. 5th European Conf. on Noise Control*, Neaples, Italy, 2003, pp. 1–6.

[14] C. May, P. Pagliarulo, and H. Janocha, "Optimisation of a magnetostrictive auxiliary mass damper," in *Proc. 10th International Conference on New Actuators*, Bremen, Germany, 2006, pp. 344–348.

[15] W. W. Morey, J. R. Dunphy, and G. Meltz, "Multiplexed fiber bragg grating sensors," *Proc. Distributed and Multiplexed Fiber Optic Sensors, SPIE*, vol. 1586.

[16] P. Pagliarulo, K. Kuhnen, C. May, and H. Janocha, "Tunable magnetostrictive dynamic vibration absorber," in *Proc. 9th International Conference on New Actuators*, Bremen, Germany, 2004, pp. 698–701.

[17] I. Perez, H. L. Cui, and E. Udd, "Acoustic emission detection using fiber bragg gratings," *Proc. SPIE*, vol. 4328.

[18] C. Z. Shia, C. C. Chanb, M. Zhangb, J. Jub, W. Jinb, Y. B. Liaoa, Y. Zhangc, and Y. Zhouc, "Simultaneous interrogation of multiple fiber bragg gratings for dynamic strain measurements," *Journal of Optoelectronics and Advanced Materials*, vol. 4, no. 4, pp. 937–941, 2002.

[19] Y. Zhao and Y. Liao, "Discrimination methods and demodulation techniques for fiber bragg grating sensors," *Opt. Lasers Eng.*, vol. 41, pp. 1–18, 2004.